*remote sensing*

*Article*

# Temporal and Spatial Variation of Land Surface Temperature and Its Driving Factors in Zhengzhou City in China from 2005 to 2020

**Shenghui Zhou [1,2], Dandan Liu [1,2], Mengyao Zhu [1,2], Weichao Tang [1,2], Qian Chi [1,2], Siyu Ye [1,2], Siqi Xu [1,2] and Yaoping Cui [1,*]**

1 Key Laboratory of Geospatial Technology for the Middle and Lower Yellow River Regions, Ministry of Education, College of Environment and Planning, Henan University, Kaifeng 475004, China
2 Key Laboratory of Integrative Prevention of Air Pollution and Ecological Security of Henan Province, Kaifeng 475004, China
* Correspondence: cuiyp@lreis.ac.cn

**Abstract:** Rapid urbanization is an important factor leading to the rise in surface temperature. How to effectively reduce the land surface temperature (LST) has become a significant proposition of city planning. For the exploration of LST and the urban heat island (UHI) effect in Zhengzhou, China, the LST was divided into seven grades, and the main driving factors of LST change and their internal relations were discussed by correlation analysis and gray correlation analysis. The results indicated that LST showed an upward trend from 2005 to 2020, and a mutation occurred in 2013. Compared with 2005, the mean value of LST in 2020 increased by 0.92 °C, while the percentage of LST-enhanced areas was 22.77. Furthermore, the spatial pattern of UHI was irregularly distributed, gradually spreading from north to south from 2005 to 2020; it showed a large block distribution in the main city and southeast in 2020, while, in the areas where woodlands were concentrated and in the Yellow River Basin, there was an obvious "cold island" effect. In addition, trend analysis and gray correlation analysis revealed that human factors were positively correlated with LST, which intensified the formation of the UHI effect, and the influence of Albedo on LST showed obvious spatial heterogeneity, while the cooling effect of vegetation water was better than that of topography. The research results can deepen the understanding of the driving mechanism of the UHI effect, as well as provide scientific support for improving the quality of the urban human settlement environment.

**Keywords:** temporal and spatial variation; land surface temperature; Zhengzhou city; urban heat island

**Citation:** Zhou, S.; Liu, D.; Zhu, M.; Tang, W.; Chi, Q.; Ye, S.; Xu, S.; Cui, Y. Temporal and Spatial Variation of Land Surface Temperature and Its Driving Factors in Zhengzhou City in China from 2005 to 2020. *Remote Sens.* **2022**, *14*, 4281. https://doi.org/10.3390/rs14174281

Academic Editors: Yuji Murayama and Ruci Wang

Received: 27 July 2022
Accepted: 26 August 2022
Published: 30 August 2022



## 1. Introduction

The continuous growth of the urban area and population has brought a series of urban environmental problems, such as the urban heat island effect, heat waves, and extreme climate. The thermal environment of cities directly affects people's quality of life, and it is closely related to the urban climate, which has always been a research hotspot [1,2]. Because the increase in land surface temperature (LST) can affect people's life and the environment in multiple ways, the urban heat island (UHI) phenomenon not only affects the local climate, vegetation growth, and air quality, but also affects people's health [3–5]. Therefore, it is a common challenge for climatologists and urban planners to formulate effective mitigation strategies for the UHI effect [6]. Determining the potential driving factors of LST is very important to reduce the urban heat island effect, promote regional sustainable development, and improve the quality of life of city dwellers [7].

According to the method of measuring temperature, the heat island can be divided into canopy layer heat island (UCL), boundary layer heat island (UBL), and surface UHI (SUHI) [8]. Among them, UCL is composed of air between rough elements (such as buildings and tree crowns), and its upper boundary is just below the roof level. UBL is located above UCL, and its lower boundary is affected by the urban surface [9]. Traditionally, the study of heat island usually depends on the on-site measurements of independent stations [10]. For example, LST is usually collected by measuring the air temperature in the urban canopy [11]. This can produce accurate and time-continuous observation results [12]; however, the spatial representation of meteorological stations limits its application, hindering the effective identification of the spatial pattern of LST. The development of remote sensing (RS) technology has provided an effective means to estimate LST from local to global scales [13,14]. Remote sensing inversion using Landsat (30 m–20 m) allows obtaining the fine LST; however, its temporal resolution is approximately every 16 days [15,16]. Moreover, the Moderate Resolution Imaging Spectroradiometer (MODIS) can provide high-resolution global LST data products, which can be directly used for mesoscale surface temperature research [17,18]. Thus, RS data can help researchers study the temporal and spatial changes of LST, and the development of RS technology has greatly promoted the progress of UHI research [19].

The interaction between influencing factors and LST leads to its spatial heterogeneity [7]; hence, exploring this internal driving relationship can provide effective strategies for alleviating the UHI phenomenon [20]. The factors that cause urban temperature change mainly include two types [21]: natural factors, such as topography, vegetation cover, and water body [22], and human factors, including urban construction intensity and socioeconomic activity index [23,24]. Furthermore, researchers have used various models and mathematical analyses to study the relationship between the spatial and temporal changes of the urban thermal environment and various index variables [25]. The main analysis models include Pearson correlation analysis, ordinary least squares regression analysis, principal component analysis, gray correlation analysis, spatial regression model (spatial lag model and spatial error model), and geographic weighted regression model [26–28]. However, existing studies typically focused on one or a few influencing factors, such as building layout, land-use change, and landscape pattern, whereas comprehensive analyses are scarce [29].

According to consensus, an increase in impermeable surfaces in cities reduces vegetation coverage and transpiration, increases the absorption of solar radiation, and leads to changes in the thermal climate and the warming of cities [30,31]. For example, Knight Teri et al. conducted a systematic review on the influence of vegetation on LST. The research showed that the surface temperature of city green space tends to be cooler than city non-green space, and the cooling effect of green space or parks can expand to 1.25 km outside its boundaries [32,33]. Furthermore, taking Shanghai as an example, Yang et al. analyzed the influence of impervious surface (IS) and vegetation cover (VC) on the intensity of the UHI. The results showed that there were obvious differences between urban and rural areas in the gradient distribution of regional land cover and surface temperature, and the heating effect of IS was more obvious than that of VC [34], whereas vegetation and water bodies had obvious cooling effects [35,36]. Liu et al. compared the influence of topography and urban form factors on the urban heat island in Chengdu and Chongqing, indicating that natural factors such as vegetation and water had a similar influence on and contribution to the UHI effect. Nevertheless, the unique topography and urban form played a key role in the difference in UHI between the two cities [37].

Owing to the many factors that can influence the formation of the UHI, a method to qualify the contributions and identify the key factors would help to alleviate the UHI effect and slow down the rising trend, especially for fast-developing cities with high construction intensity and continued growth of non-green spaces [38]. In order to explore the internal relationship between the driving factors of the UHI effect from two aspects of natural and human factors, we chose Zhengzhou as the research area. Zhengzhou is the main economic development center of Henan Province in China; thus, the large number of human activities can easily cause the phenomenon of UHI in this area [39]. However, there has been little research on SUHI in Zhengzhou, while mostly single driving factors were investigated, long timeseries of remote sensing data were not evaluated [40]. Through the analysis of the temporal and spatial variation of land surface temperature and the driving factors of the UHI effect in Zhengzhou, the results of this research can make up for the deficiency of this field, providing a theoretical basis and decision support for the improvement of urban construction and environmental quality of human settlements, as well as providing a reference for future urban planning and design in Zhengzhou.

## 2. Materials and Methods

### *2.1. Study Area*

The study area was Zhengzhou (112°42′E–114°14′E, 34°16′N–34°58′N), the capital of Henan Province in China, located in the hinterland of China, with the Yellow River in the north, Huanghuai Plain in the southeast, and Songshan Mountain in the west. As shown in Figure 1, the terrain is high in the west and low in the east. D1-D12 are districts, which are Huiji, Zhongyuan, Jinshui, Guancheng Hui, Erqi, Xingyang, Shangjie, Gongyi, Zhongmu, Xinmi, Dengfeng and Xinzheng respectively. Zhengzhou's total population in 2020 reached $1.2601 \times 10^7$, representing a densely populated mega city (Statistics Bureau of Zhengzhou, http://tjj.zhengzhou.gov.cn/, accessed on 20 May 2022). In addition, Zhengzhou is located at the intersection of the Beijing–Guangzhou urban development belt and the Longhai urban development belt. It is the central city of the Central Plains urban agglomeration, an important node city in the Zheng–Bian–Luo Industrial Corridor, and one of the most representative cities in urban development in China.

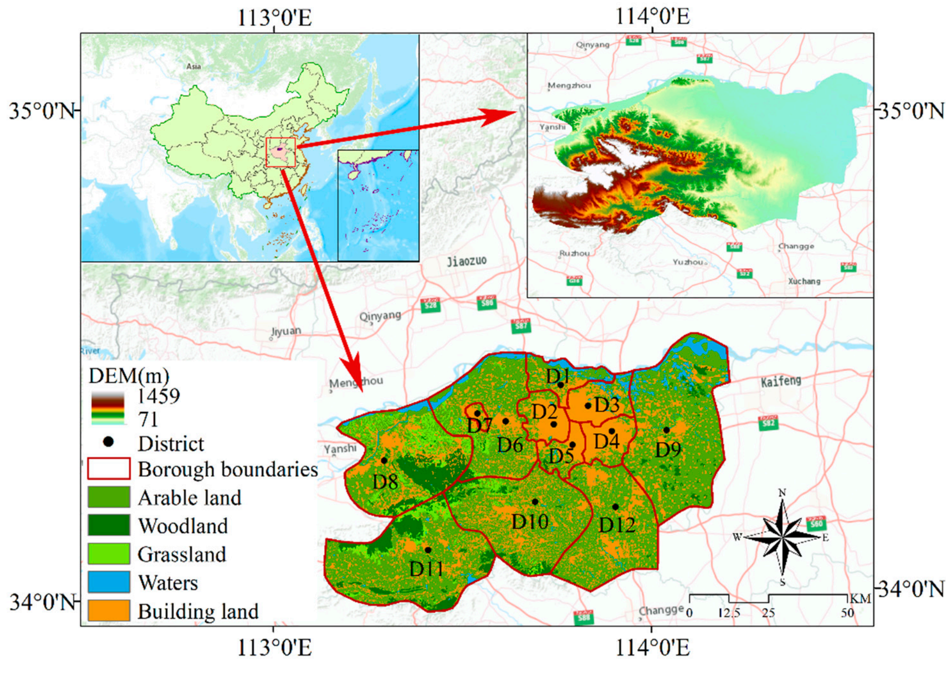


**Figure 1.** The location map of Zhengzhou.

### *2.2. Data Resources*

The DEM (digital elevation model) data and land-use data in 2020 were obtained from the Resource and Environmental Science Data Center of China, with a spatial resolution of 205 m and 30 m, respectively (http://www.resdc.cn, accessed on 5 March 2022 and 14 March 2022). The Landsat8 OLI_TIRS remote sensing image of 22 May 2020 came from the geospatial data cloud with a cloud content of 6.12% and a spatial resolution of 30 m. The NDISI (normalized difference impervious surface index), NDBBI (normalized difference bareness and built-up index), and MNDWI (modified normalized difference water index) were calculated using the Landsat8 OLI_TIRS remote sensing image (downloaded from http://www.gscloud.cn/#page1/1, accessed on 8 March 2022). The LST, NDVI (normalized difference vegetation index), and Albedo MODIS data products were downloaded from https://modis.gsfc.nasa.gov (accessed on 1 March 2022 and 14 March 2022). The

MODIS data characteristics are shown in Table 1. Zhengzhou POI data in 2020 came from Gaode map (https://ditu.amap.com, accessed on 15 March 2022), including 11 points of interest: catering, living and entertainment, shopping centers, public service facilities, scenic spots, companies and enterprises, government agencies, medical care, commercial housing, accommodation, and sports and leisure, which could be used to represent socioeconomic activities.

**Table 1.** MODIS data items and descriptions.

| Data Items | Spatial Resolution | Time Resolution | Data Resource |
|---|---|---|---|
| LST | 1 km | 8 days | MYD11A2 |
| NDVI | 250 m | 16 days | MYD13Q1 |
| Albedo | 500 m | Daily | MCD43A3 |

In this study, the timeseries data mainly included MDOSI LST data from 2005 to 2020, which were used to analyze the trend of surface temperature in Zhengzhou. The cross-sectional data included the Landsat 8 OLI_TIRS remote sensing image, which was used to calculate the NDISI, NDBBI, and MNDWI. In addition, the NDVI, DEM, Albedo, and POI were used to analyze the driving relationship between LST and the influencing factors. In order to study the relationship between LST and the raster data of influencing factors in Zhengzhou, the raster-to-point tool in ArcGIS was used to convert LST raster data into point data, and then the influencing factor data of corresponding points were extracted using a multivalue extraction to point tool.

### *2.3. Research Methodology*

#### 2.3.1. Nonparametric Mann–Kendall Trend Test

The nonparametric Mann–Kendall trend test (M–K test) [41,42] was used to test changes in LST over time from 2005 to 2020. The principle is described below [43].

(1) According to the timeseries $X_1, X_2, \ldots, X_n$, construct an ordered sequence as follows:

$$S_K = \sum_{i=1}^{K} R_i,\ R_i = \begin{cases} 1,\ X_i > X_j \\ 0,\ X_i \le X_j \end{cases},\ (K = 1,\ 2, 3, \ldots, n). \tag{1}$$

(2) Calculate the mean and variance of $S_K$ as follows:

$$\mathrm{E}(S_K) = n(n+1)/4. \tag{2}$$

$$\mathrm{Var}(S_K) = n(n-1)(2n+5)/72. \tag{3}$$

(3) Standardize $S_K$ as follows:

$$UF_K = \frac{S_K - E(S_K)}{\sqrt{Var(S_K)}}(K = 1, 2, \ldots, n). \tag{4}$$

Here, $UF_k$ is the standard normal distribution, given a significance level $\alpha$ (generally $\alpha$ = 0.05, $UF_\alpha$ = $\pm$1.96); $|UF_k| > U_\alpha$ indicates a significant trend change. $UF_k > 0$ indicates an upward trend, and vice versa. The X-series is inverted to obtain a new timeseries $X_n, X_{n-1}, \ldots, X_1$, and the above process is repeated to obtain $UB_K = -UF_K$, where $UB_1 = 0, K = n, n-1, \ldots, 1$.

#### 2.3.2. Calculation of Surface Information Index

NDISI can be used to represent the impervious surface. Impervious surface refers to artificial ground objects that are impervious to water, and its changing trend can directly or indirectly evaluate the development of a city. The area of impervious surface in a city increases greatly, which can lead to serious urban waterlogging, the UHI effect, and environmental resource pollution [44]. The calculation equation of NDISI is shown below [26,45].

$$NDISI = \frac{TIRS1 - (MNDWI + N + SWIR1)/3}{TIRS1 + (MNDWI + N + SWIR1)/3}. \quad (5)$$

MNDWI is an improved normalized difference water body index, which is used to represent water body information.

$$MNDWI = \frac{G - SWIR1}{G + SWIR1}. \quad (6)$$

NDBBI can be used to obtain the information of urban bare land and built land.

$$NDBBI = \frac{1.5SWIR2 - (N + G)/2}{1.5SWIR2 + (N + G)/2}, \quad (7)$$

where $G$, $N$, $SWIR1$, $SWIR2$, and $TIRS1$ correspond to bands 3, 5, 6, 7, and 10, respectively, in Landsat8 OIL-TIR.

Land surface albedo represents the reflective ability of the Earth's surface to solar radiation, and its magnitude is influenced by many factors such as solar altitude angle, land-use type and coverage, and surface roughness. It is an important dynamic dimensionless surface parameter to study the balance of land energy and global climate change [46].

Slope refers to the angle between the actual ground and the horizontal plane, which was calculated using the slope analysis tool in ArcGIS10.5 software.

The socioeconomic activity index can directly reflect the development level of urban areas and indirectly represent the impact of human activities on UHI. In this study, it was expressed using the POI kernel density.

#### 2.3.3. Correlation Analysis and Linear Trend Analysis

In statistics, the Pearson correlation coefficient, also known as the Pearson product-moment correlation coefficient (PPMCC), is used to measure the relationship between two variables $X$ and $Y$, with values ranging from $-1$ to +1, and it is widely used in academic research to measure the strength of linear correlation between two variables [47]. The Pearson correlation coefficient between two variables is defined as the quotient of the covariance of these two variables and the product of their standard deviations.

$$\rho_{X,Y} = \frac{cov(X,Y)}{\sigma_X \sigma_Y} = \frac{E[(X - \mu X)(Y - \mu Y)]}{\sigma_X \sigma_Y}. \quad (8)$$

Equation (8) defines the overall correlation coefficient. The Pearson correlation coefficient can be obtained by estimating the covariance and standard deviation of the sample, which is commonly represented by r.

$$\mathrm{r} = \frac{\sum_{i=1}^{n} (X_i - \overline{X})(Y_i - \overline{Y})}{\sqrt{\sum_{i=1}^{n} (X_i - \overline{X})^2} \sqrt{\sum_{i=1}^{n} (Y_i - \overline{Y})^2}}. \quad (9)$$

Furthermore, r can be estimated using the standard score mean of $(X_i,\ Y_i)$ sample points, and the equivalent expression of Equation (9) can be obtained as follows:

$$\mathrm{r} = \frac{1}{n-1} \sum_{i=1}^{n} \left( \frac{X_i - \overline{X}}{\sigma X} \right) \left( \frac{Y_i - \overline{Y}}{\sigma Y} \right), \quad (10)$$

where $\frac{X_i - \overline{X}}{\sigma X}$, $\overline{X}$, and $\sigma X$ are the standardized variable, sample mean, and sample standard deviation, respectively.

In this study, Pearson correlation analysis was used to explore the correlation and interaction between LST and influencing factors, and SPSS software was used to analyze the results.

#### 2.3.4. Gray Relational Analysis Model

Gray correlation analysis [48,49] is a gray process based on the gray system, which compares the timeseries between factors to determine the most influential leading factors. The magnitude of the correlation degree is an external expression of the mutual influence and interaction among factors, and the order of the correlation degree reflects the relative influence of each factor on the reference factor. The principle of gray relational degree analysis is described below [27].

(1) Suppose the original timeseries $X_i = \{X_i(K)|K = 1,\ 2\ldots,\ n;\ i = 0,\ 1,\ 2,\ldots,\ m-1\}$ is composed of $n$ evaluation samples of $m$ evaluation indicators. First, the original timeseries is averaged to obtain the sequence $X_i$.

$$X_i(k) = \frac{X_i(k)}{\overline{X_i}}, K = 1,\ 2\ldots,\ n;\ i = 0,\ 1,\ 2,\ldots,\ m-1, \tag{11}$$

where $X_0$ is the reference sequence, and the others are comparison sequences; $i \neq 0$ unless otherwise specified.

(2) Calculate the absolute difference between $X_0$ and $X_i$ at time $\boldsymbol{K}$.

$$\Delta_i(K) = |X_0(K) - X_i(K)|, i = 1, 2, \ldots, m-1. \tag{12}$$

(3) Calculate the correlation coefficient $\xi_i(K)$.

$$\xi_i(K) = \frac{\min_i \min_k \Delta_i(K) + \rho \max_i \max_k \Delta_i(K)}{\Delta_i(K) + \rho \max_i \max_k \Delta_i(K)}, \tag{13}$$

where $\min_i \min_K$ is the minimum difference between two poles, and $\max_i \max_K$ is the maximum difference between two poles. Furthermore, as the resolution coefficient, $\rho \in (0, 1)$, a smaller $\rho$ indicates a greater resolution, which is generally 0.5.

(4) Calculate the gray correlation degree $\gamma_i$.

$$\gamma_i = \frac{1}{n} \sum_{k=1}^{n} \xi_i(K). \tag{14}$$

By sorting the gray correlation degree $\gamma_i$ in order of magnitude, the relative influence degree of various factors on the reference factor can be obtained. The framework of this study is shown in Figure 2.

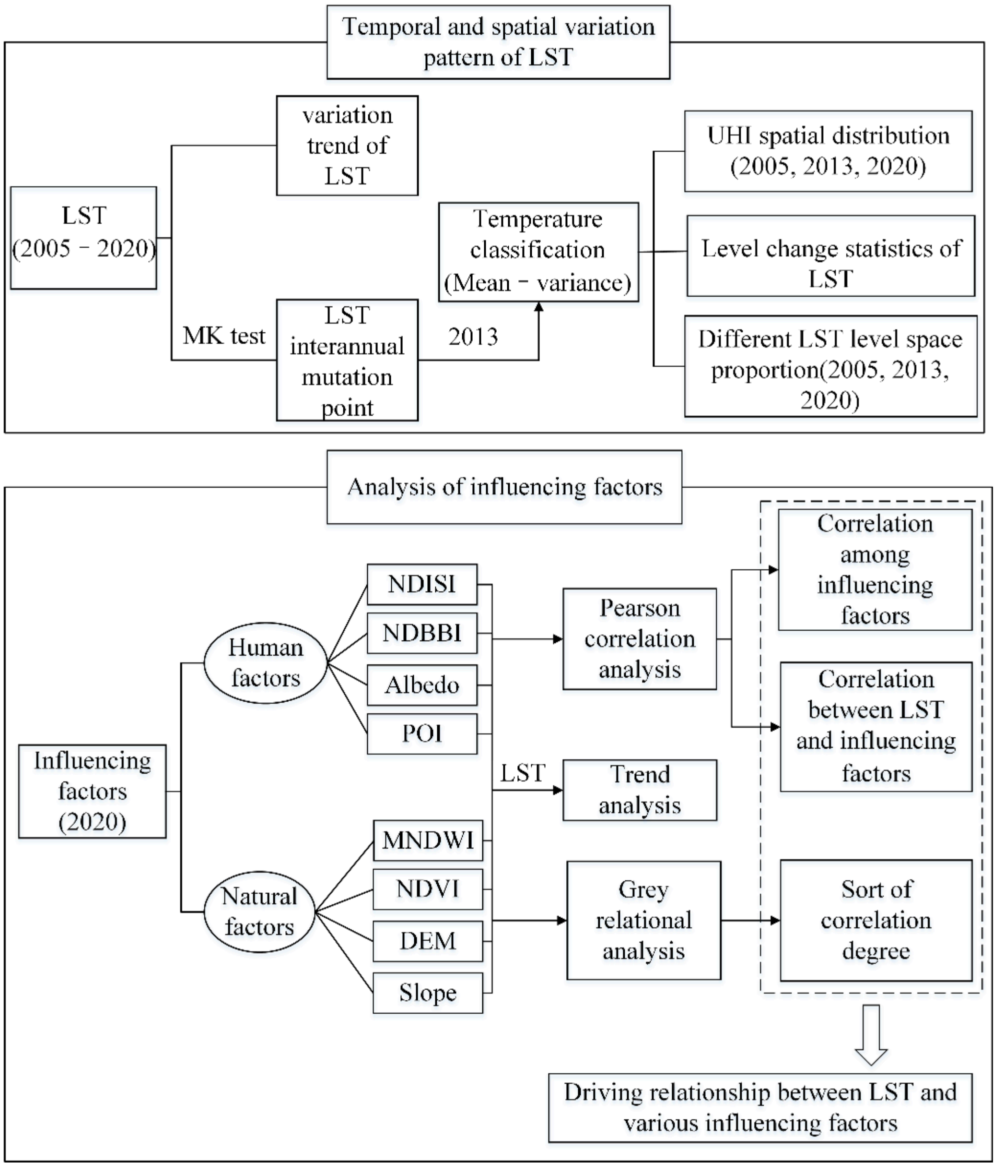


**Figure 2.** Framework of this study.

## 3. Results

### *3.1. Characteristics of Urban Thermal Environment Evolution*

#### 3.1.1. Interannual Variation Characteristics of LST

As can be seen from Figure 3A, the interannual variation trend of surface temperature in Zhengzhou from 2005 to 2020 was small, and the variation trends of the mean and maximum values were similar, but they all showed an overall upward trend. From 2005 to 2020, the mean value of LST increased by 0.92 °C, and the maximum value increased by 0.85 °C. Moreover, the mean value and maximum value both reached the maximum in 2019 (26.59 °C and 31.58 °C, respectively).

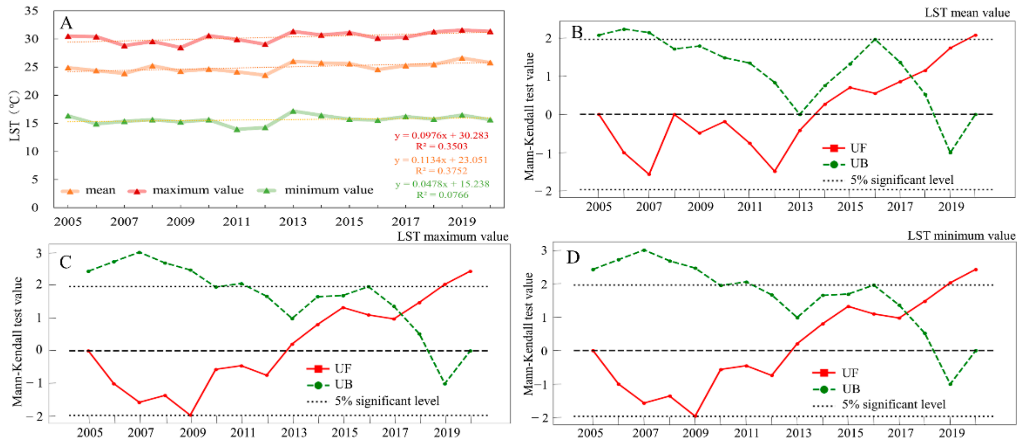


**Figure 3.** Variation of LST in Zhengzhou from 2005 to 2020 and M–K test values: (**A**) interannual variation; (**B**) M–K mean; (**C**) M–K maximum; (**D**) M–K minimum (yellow: mean, red: maximum, green: minimum).

Figure 3B–D show the M–K test values of the interannual variation of the land surface temperature in Zhengzhou. As can be seen from Figure 3B–D, the UF curve was in a downward trend before 2013, and the trend change was not obvious. In the second half of 2013, it began to show an upward trend, while there was a significant upward trend in the second half of 2019. The UF curve of LST maximum and minimum values began to show an upward trend in 2013, while, after 2019, the upward trend was significant.

#### 3.1.2. Surface Temperature Classification

To identify the reason for the difference in LST in the study area, the mean-variance method was used to classify the LST into seven categories, as shown in Table 2: extremely high temperature, high temperature, relatively high temperature, medium temperature, relatively low temperature, low temperature, and extremely low temperature [26]. The first three categories were considered UHI zones in this study.

**Table 2.** Classification of LST.

| Temperature Rating | Extremely High-Temperature Zone | High-Temperature Zone | Relatively High -Temperature Zone | Medium-Temperature Zone | Relatively Low-Temperature Zone | Low-Temperature Zone | Extremely Low-Temperature Zone |
|---|---|---|---|---|---|---|---|
| Temperature range | $t \geq u + 2.5$ std | $u + 1.5$ std $\leq t <$ $u + 2.5$ std | $u + 0.5$ std $\leq t <$ $u + 1.5$ std | $u - 0.5$ std $\leq t <$ $u + 0.5$ std | $u - 1.5$std $\leq t <$ $u - 0.5$ std | $u - 2.5$ std $\leq t < u$ $- 1.5$ std | $t < u - 2.5$ std |

Note: u represents the mean value of LST; std represents the standard deviation of LST.

#### 3.1.3. Spatial Evolution Characteristics of Urban Thermal Environment

Figure 4 shows the spatial evolution of the urban heat island in Zhengzhou in 2005, 2013, and 2020. As shown in Figure 4, the UHI area was irregular and gradually spread from north to south, and it was distributed in the main city and southeast in 2020. High temperature mainly occurred in the main city areas and densely built areas, while low temperature was most concentrated in the areas covered by rivers, grasslands, and woodlands. The spatial distribution characteristics of UHI were similar in the three periods, showing an obvious "cold island" effect in the Yellow River basin and the concentrated distribution area of woodland. The extremely high-temperature zone, relatively high-temperature zone, and high-temperature zone continued to expand along densely populated areas from 2005 to 2020.

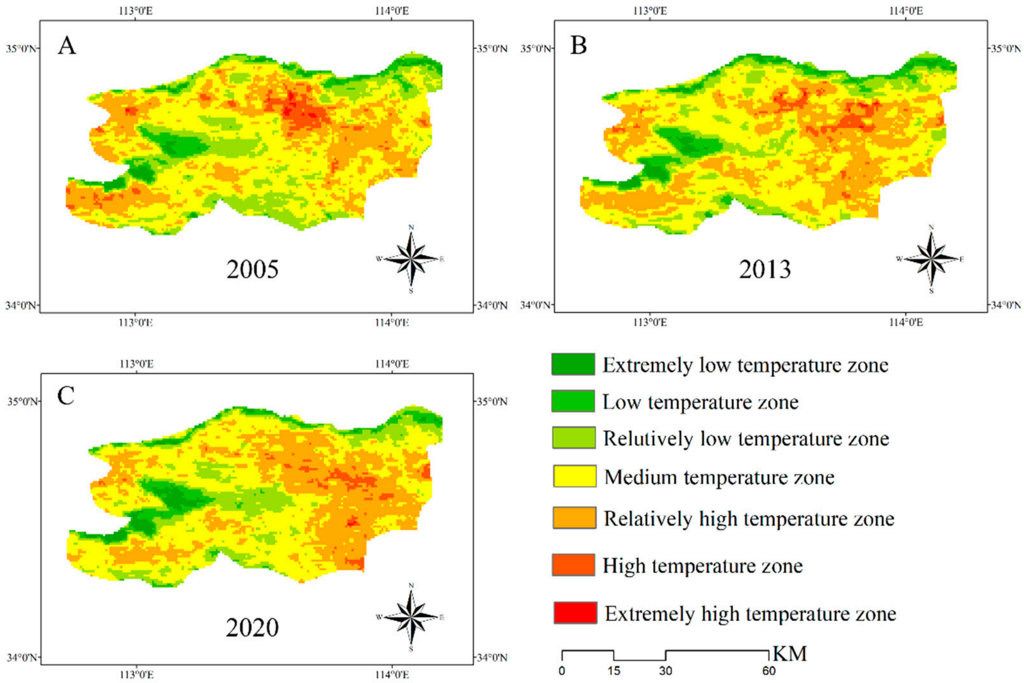


**Figure 4.** Spatial evolution of UHI in Zhengzhou in 2005, 2013, and 2020: (**A**) 2005, (**B**) 2013, (**C**) 2020.

### 3.1.4. Temporal Evolution Characteristics of Urban Thermal Environment

As shown in Table 3, the changes in LST grades in 2005, 2013, and 2020 were calculated. Table 3 indicates that the percentage area with weakened LST grades in Zhengzhou from 2005 to 2020 was 23.51%, while unchanged areas accounted for 53.72%, and the enhanced areas accounted for 22.77%. From 2005 to 2013, 20.83% of the area was represented by weakened LST grades, in contrast to 57.48% for unchanged areas and 21.69% for enhanced areas. From 2013 to 2020, the percentage area with weakened LST grades was 21.20%, an increase of 0.37% over the previous period. The percentage area with a constant LST level was 58.43%, which was 0.95% higher compared to the previous period. The percentage area with an enhanced LST level was 20.37%, which was 1.32% lower than that of the previous period. Through the above analysis, it was found that, in the last 15 years, the LST grade in Zhengzhou changed to different degrees. Compared with 2013–2020, the proportion of areas with weakened and unchanged LST grades in 2005–2013 showed an upward trend, while the enhanced areas showed a downward trend.

**Table 3.** LST grade change detection statistics in 2005–2013, 2013–2020, and 2005–2020.

| Category | Range | 2005–2013 | | 2013–2020 | | 2005–2020 | |
|---|---|---|---|---|---|---|---|
| | | Grade Percentage | Class Percentage | Grade Percentage | Class Percentage | Grade Percentage | Class Percentage |
| Weaken | −6 | 0.00% | 20.83% | 0.00% | 21.20% | 0.00% | 23.51% |
| | −5 | 0.00% | | 0.00% | | 0.00% | |
| | −4 | 0.00% | | 0.00% | | 0.00% | |
| | −3 | 0.00% | | 0.01% | | 0.00% | |
| | −2 | 1.24% | | 0.57% | | 1.07% | |
| | −1 | 19.59% | | 20.62% | | 22.44% | |
| Constant | 0 | 57.48% | 57.48% | 58.43% | 58.43% | 53.72% | 53.72% |
| Enhance | 1 | 20.46% | 21.69% | 19.73% | 20.37% | 20.95% | 22.77% |
| | 2 | 1.17% | | 0.63% | | 1.70% | |
| | 3 | 0.06% | | 0.01% | | 0.12% | |
| | 4 | 0.00% | | 0.00% | | 0.00% | |
| | 5 | 0.00% | | 0.00% | | 0.00% | |
| | 6 | 0.00% | | 0.00% | | 0.00% | |

In order to better research the temporal and spatial evolution of the urban heat island in Zhengzhou, the proportions of different temperature grades in 2005, 2013, and 2020 were calculated. As shown in Table 4, in 2005, 2013, and 2020, the proportions of extremely low-temperature area, low-temperature area, and relatively high-temperature area in Zhengzhou showed an upward trend, with the proportion of relatively high-temperature area increasing by 4.03%. On the other hand, extremely high-temperature, high-temperature, and low-temperature areas showed a downward trend, with the high-temperature and relatively low-temperature areas decreasing by 1.72% and 3.22%, respectively, whereby the high-temperature area, extremely high-temperature area, and relatively low-temperature area transformed into relatively high-temperature areas. By 2020, the proportion of the relatively high-temperature zone reached 30.47%, and it was concentrated in the southeast, with a small distribution in the west and southwest. In addition, in 2005, 2013, and 2020, the heat island area accounted for 30.88%, 32.93%, and 32.96%, respectively, showing a 2.08% increase from 2005 to 2020.

**Table 4.** Proportion of different temperature grades (%) in 2005, 2013, and 2020.

| Year | Extremely High | High | Relatively High | Medium | Relatively Low | Low | Extremely Low |
|---|---|---|---|---|---|---|---|
| 2005 | 0.27 | 4.17 | 26.44 | 43.44 | 18.02 | 5.63 | 2.03 |
| 2013 | 0.12 | 3.01 | 29.80 | 43.98 | 13.8 | 6.61 | 2.67 |
| 2020 | 0.04 | 2.45 | 30.47 | 43.48 | 14.80 | 6.00 | 2.78 |

## *3.2. Analysis of Driving Factors of Urban Thermal Environment*

### 3.2.1. Correlation Analysis

According to the analysis of the thermal environment effect in Zhengzhou in 2005, 2013, and 2020, the heat island effect was the most obvious in 2020. Therefore, the influencing factors were analyzed on the basis of the LST data in 2020. In this research, according to the city location and terrain characteristics of Zhengzhou, the relevant human and natural factors were selected for analysis, as shown in Table 5. Among them, the human factors included urban construction intensity (NDISI, NDBBI, and Albedo) and the socioeconomic activity index (POI kernel density), while the natural factors included water body, vegetation, and topographic landforms.

**Table 5.** Influencing factors of urban thermal environment.

| First Level Indicators | Second Level Indicators | Third Level Indicators |
|---|---|---|
| Natural factors | Water body | MNDWI |
| | Vegetation and | NDVI |
| | Topographic features | Slope |
| | | DEM |
| Human factors | Intensity of urban construction | NDISI |
| | | NDBBI |
| | | Albedo |
| | Socioeconomic activities | POI |

The LST data and impact factor data of the study area were extracted in GIS using the grid turning point tool before conducting correlation analysis. The Pearson correlation coefficients among indices (Table 6) and the Pearson correlation coefficients between LST and each index (Table 7) were obtained. It can be seen from Tables 6 and 7 that the factors influencing LST in Zhengzhou showed weak and moderate correlation at the 0.01 significance level, and the absolute value range of the correlation coefficient $R$ was between 0.045 and 0.761. Moreover, the eight influencing factors were correlated with LST at the 0.01 significance level, with correlation coefficients $|R| \in [0.027, 0.574]$. Among them, as shown in Table 7, LST had a significant negative correlation with DEM, MNDWI, NDVI, and Slope, indicating that vegetation, water, and high terrain had a cooling effect, which could alleviate the UHI effect. LST had a significant positive correlation with POI, NDBBI, NDISI, and Albedo. The results show that human activities and the intensity of urban construction affected the urban thermal environment, and the heat generated by high-intensity human activities did not dissipate well, causing the urban heat island phenomenon.

**Table 6.** Pearson correlation among influencing factors.

| Factor | NDVI | MNDWI | DEM | Slope | NDISI | NDBBI | Albedo | POI |
|---|---|---|---|---|---|---|---|---|
| NDVI | 1 | −0.379 ** | 0.368 ** | 0.330 ** | −0.301 ** | −0.385 ** | −0.659 ** | −0.338 ** |
| MNDWI | −0.379 ** | 1 | −0.241 ** | −0.197 ** | 0.687 ** | −0.293 ** | 0.249 ** | 0.182 ** |
| DEM | 0.368 ** | −0.241 ** | 1 | 0.761 ** | −0.208 ** | −0.330 ** | −0.701 ** | −0.136 ** |
| Slope | 0.330 ** | −0.197 ** | 0.761 ** | 1 | −0.185 ** | −0.349 ** | −0.641 ** | −0.110 ** |
| NDISI | −0.301 ** | 0.687 ** | −0.208 ** | −0.185 ** | 1 | −0.045 ** | 0.136 ** | 0.187 ** |
| NDBBI | −0.385 ** | −0.293 ** | −0.330 ** | −0.349 ** | −0.045 ** | 1 | 0.430 ** | 0.057 ** |
| Albedo | −0.659 ** | 0.249 ** | −0.701 ** | −0.641 ** | 0.136 ** | 0.430 ** | 1 | 0.180 ** |
| POI | −0.338 ** | 0.182 ** | −0.136 ** | −0.110 ** | 0.187 ** | 0.057 ** | 0.180 ** | 1 |

Note: ** indicates that the correlation was significant at the level of 0.01 (detection < 0.01).

**Table 7.** Correlation coefficients between factors and LST.

| — | NDVI | MNDWI | DEM | Slope | NDISI | NDBBI | Albedo | POI |
|---|---|---|---|---|---|---|---|---|
| LST | −0.301 ** | −0.027 ** | −0.574 ** | −0.568 ** | 0.141 ** | 0.457 ** | 0.527 ** | 0.195 ** |

Note: ** indicates that the correlation was significant at the level of 0.01 (detection < 0.01).

Figure 5 reflect the linear relationship between LST and various influencing factors. As shown in Figure 5, LST showed a downward trend under the action of NDVI, MNDWI, DEM, and Slope, with the downward trends of DEM and Slope being more obvious ($R^2$ = 0.3297 and 0.3222, respectively). Furthermore, LST was increased under the action of NDISI, NDBBI, Albedo, and POI. The trend analysis was consistent with the correlation analysis. Furthermore, the interaction between LST and Albedo showed spatial heterogeneity due to the complex effects of surface cover, elevation, and other factors [50]. Generally speaking, LST and Albedo were on the rise, which was related to the rise in surface temperature, the increase in vegetation and soil water stress, and the decrease in water content, which led to the increase in surface albedo. Moreover, the rise in surface temperature, vegetation growth, and increase in reflectivity in the near-infrared band also led to a significant increase in surface albedo. However, LST and Albedo showed a downward trend in the interval of 0.2–0.3, and these points were mainly distributed in rivers and grasslands. With the increase in Albedo, the light radiation energy absorbed by the surface decreased, resulting in a decrease in LST (Figure 5G).

Figure 6 shows the spatial distribution of each index in Zhengzhou. NDVI was basically consistent with the vegetation distribution in the study area. The improved MNDWI distribution was basically consistent with the water distribution in Zhengzhou. The southwest elevation of Zhengzhou is large, and the slope had a positive correlation with the elevation. The spatial distribution of NDBBI, Albedo, and NDISI was related to the type of urban underlying surface, with high values concentrated in the built-up areas. High POI values were concentrated in the main city area.

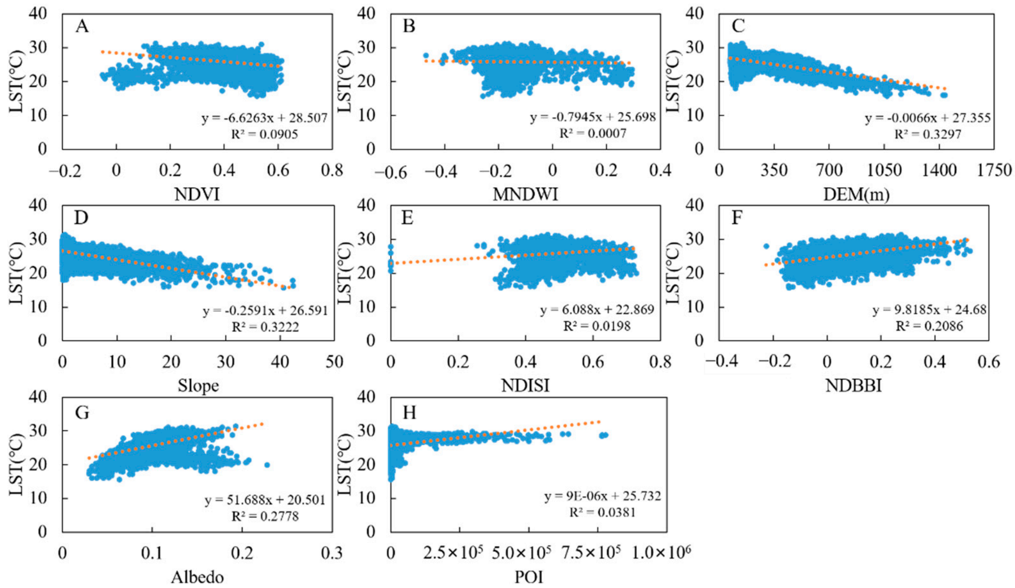

**Figure 5.** Linear relationship between influencing factors and LST in Zhengzhou: (**A**) NDVI; (**B**) MNDWI; (**C**) DEM; (**D**) Slope; (**E**) NDISI; (**F**) NDBBI; (**G**) Albedo; (**H**) POI.

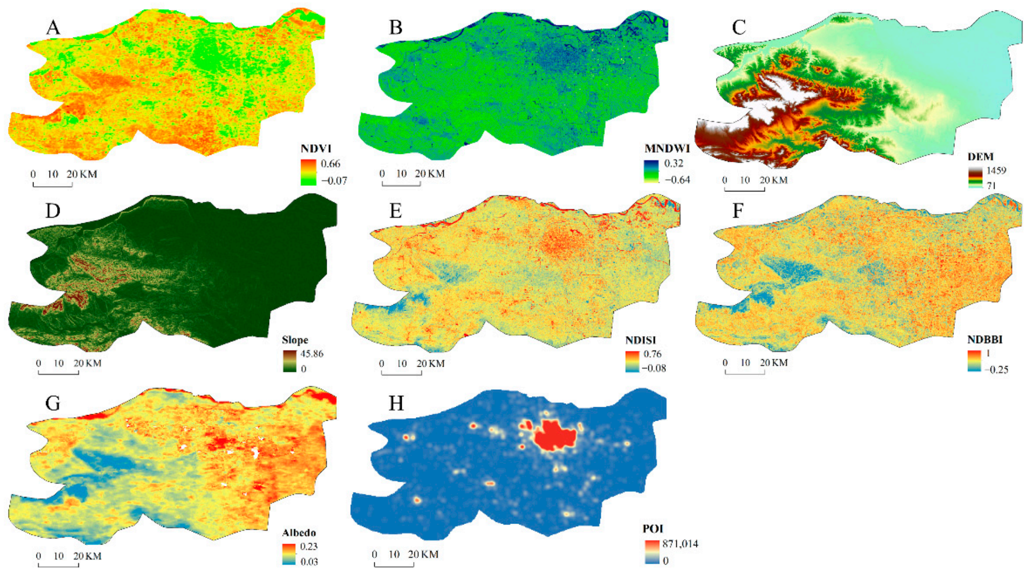

**Figure 6.** Spatial distribution of indicators in Zhengzhou: (**A**) NDVI; (**B**) MNDWI; (**C**) DEM; (**D**) Slope; (**E**) NDISI; (**F**) NDBBI; (**G**) Albedo; (**H**) POI.

### 3.2.2. Gray Correlation Analysis

The correlation between the above eight indices and LST was analyzed, but the correlation coefficient does not represent the contribution of each index to the change in LST. Because the correlation coefficient between variables indicates how close they are to each other, when there are many factors, this correlation only reflects their compound relationship, while it does not represent the relative influence degree or effect of each factor on the change in heat island intensity [27,51]. Thus, in order to reveal the contribution of the eight indices to LST, this study took LST as the reference series and the other eight influencing factors as the comparison series, before calculating their gray correlation degree. The results are shown in Table 8.

**Table 8.** The correlation of LST with each index.

| Impact Factor | Correlation | Sort |
|---|---|---|
| NDISI | 0.99978 | 1 |
| Albedo | 0.99965 | 2 |
| NDVI | 0.99943 | 3 |
| MNDWI | 0.99919 | 4 |
| DEM | 0.99834 | 5 |
| NDBBI | 0.99831 | 6 |
| Slope | 0.99718 | 7 |
| POI | 0.98030 | 8 |

As can be seen from Table 8, there were some differences in the order of correlation coefficient between these eight indices and LST. Because the correlation degree in gray theory reflects the correlation degree of independent variables compared with dependent variables, it can explain the dependent variable through the transmission of other independent variables without considering one independent variable [27,52]. In addition, the correlation degrees between the eight indices and LST were all above 0.98, and the difference between the maximum value and minimum value was only 0.01948. This shows that, although the indices were ranked sequentially, they were highly correlated with LST. According to the order of correlation degree, the contribution degree of the urban construction intensity and vegetation water body to LST change was the largest, and the correlation degree was above 0.999. This indicted that these four factors had a high degree of synchronous change with LST in the process of development and change; therefore, they were the most direct factors leading to the change in heat island intensity. However, the correlation of DEM, NDBBI, and Slope with LST was between 0.996 and 0.999, indicating that these three factors contributed extensively to the change in urban LST. In fact, NDBBI was also indirectly reflected in NDISI. Moreover, the correlation degree of social economic activity index POI was the lowest, but its value was 0.98030, indicating that it also had a high impact on the change in LST.

## 4. Discussion

Urbanization leads to changes in urban atmospheric dynamic characteristics and land use/land cover types, thereby affecting the formation of the urban heat island effect [26]. Furthermore, the spatial heterogeneity of LST may be affected by topography in different areas [36]. The terrain of Zhengzhou is high in the west and low in the east. The results showed that the UHI effect in Zhengzhou had obvious spatial differentiation characteristics. Cold islands mainly occurred in the west, densely forested areas, and Yellow River Basin, whereas heat islands were mainly distributed in southeast plains and built-up areas, where the population was dense, and the proportion impervious water surfaces rapidly increased, thus hindering the dissipation of heat and forming a large area of high temperature. Therefore, LST had the characteristics of "low on the periphery and high in the middle".

A city is a complex dynamic system composed of social connections, human activities, and infrastructure. The UHI is the result of multiple factors of local climate and human activities [26]. The interaction between surface temperature and vegetation dynamics under different land-cover types leads to changes in the spectral radiance and texture of surface temperature, resulting in the spatial pattern of urban heat island [8]. Moreover, impervious surfaces (such as concrete, cement, and asphalt) usually show lower emissivity and higher heat capacity than natural surfaces [53]. In the analysis of LST driving factors in Zhengzhou, the urban construction intensity contributed the most to the formation of the UHI effect, and the expansion of the urban impermeable water surface increased the absorption of solar radiation, resulting in a rapid increase in the land surface temperature [54]. On the other hand, vegetation and water bodies are effective tools to restrain the UHI effect and reduce the LST [55], while controlling the impervious surface percentage of construction land at a low level (e.g., below ~49%) can effectively alleviate the impact of the SUHI [54]. Therefore, this represents a strategic measure to effectively alleviate the UHI effect and build an ecologically livable city by controlling the proportion of impermeable water surface, increasing the urban vegetation coverage area, and rationally utilizing the water distribution, topography, and other features.

This research used multiple sources of data to study the temporal and spatial distribution characteristics and driving factors of Zhengzhou's thermal environment, while correlation analysis, trend analysis, and gray correlation analysis were applied to reveal the correlation between natural and human influencing factors. This study can be helpful for planners to understand the causes and mitigation measures of the UHI effect in Zhengzhou, through reasonably controlling the layout of buildings, effectively utilizing the distribution of vegetation and water, and actively guiding urban ventilation, so as to achieve the purpose of reducing LST and building a livable city. From this perspective, follow-up research can enable planners to more comprehensively understand the driving factors of the UHI effect.

## 5. Conclusions

Exploring the mitigation strategies of land surface temperature in Zhengzhou is of great significance for sustainable development and environmental quality. In this study, the main conclusions were as follows:

(1) The annual changes in LST in Zhengzhou from 2005 to 2020 were small, with a mutation point in 2013. Furthermore, compared with 2005, in 2020, the mean value of LST increased by 0.92 °C, the percentage of LST-enhanced areas was 22.77%, and the area of the heat island increased by 2.08%.

(2) The spatial pattern of the urban heat island showed an irregular block distribution, gradually spreading from north to south from 2005 to 2020; in 2020, there was a large block distribution in the main city and southeast. In addition, high temperatures mainly occurred in the main urban areas and densely built areas, whereas there was an obvious "cold island" effect in the concentrated distribution areas of forest land and the Yellow River basin.

(3) The results of correlation analysis, trend analysis, and gray correlation analysis showed that human factors (NDISI, NDBBI, Albedo, and POI) were positively correlated with LST, which intensified the formation of the UHI effect, with the influence of Albedo on LST showing obvious spatial heterogeneity. Natural factors (NDVI, MNDWI, DEM, and Slope) were negatively correlated with LST. Among them, the intensity of urban construction had the highest contribution to the formation of the UHI effect, and the cooling effect of vegetation and water was better than that of topography.

Generally, the UHI strength of Zhengzhou City revealed a significant increasing trend from 2005 to 2020. Zhengzhou's altitude is high in the west and low in the east, and there was a negative correlation of DEM and Slope with LST. Therefore, it is possible to reasonably control the layout of urban buildings as a function of the topography, such that mountain wind and cold air can smoothly enter the city and accelerate the air flow. In addition, the cooling effect of vegetation and water was obviously better than that of topography. In urban planning, connecting vegetation, water, and road networks in the urban ventilation corridor represents an effective measure to alleviate the urban heat island effect. As the economic center of Henan Province, Zhengzhou's comprehensive influence of human activities and urban construction intensity on the urban underlying surface is an important factor mediating the UHI. These results can help decision makers and urban planners to make rational and scientific decisions and promote the sustainable development of cities such as Zhengzhou in the future.

**Author Contributions:** Conceptualization, S.Z., Y.C. and D.L.; methodology, D.L. and S.Z.; software, M.Z.; validation, M.Z., D.L., W.T., S.X. and S.Y.; formal analysis, Q.C. and S.Z.; investigation, S.Z. and D.L.; resources, S.Z.; data curation, D.L.; writing—original draft preparation, D.L. and S.Z.; writing—review and editing, S.Z. and D.L.; visualization, D.L., M.Z., W.T., S.X. and S.Y.; supervision, S.Z. and Y.C.; project administration, Y.C. and S.Z.; funding acquisition, S.Z. The first two authors contributed equally to this work and should be considered co-first authors. All authors have read and agreed to the published version of the manuscript.

**Funding:** This research was funded by the National Natural Science Foundation of China (grant numbers 42005102 and 42071415), the Qinghai Science and Technology Department Project (grant number 2020-ZJ-711), the Second Tibetan Plateau Comprehensive Scientific Expedition (grant number 2019QZKK0104), the National Key Research and Development Program of China (grant number 2021YFE0106700), and the Outstanding Youth Foundation of Henan Natural Science Foundation (grant number 202300410049).

**Data Availability Statement:** The land-use data and DEM data in 2020 were obtained from the Resource and Environmental Science Data Center of China (http://www.resdc.cn, accessed on 14 March 2022 and 5 March 2022). The Landsat8 OLI_TIRS remote sensing image of 22 May 2020 was obtained from the geospatial data cloud (http://www.gscloud.cn/#page1/1, accessed on 8 March 2022). LST and NDVI, Albedo MODIS data products were download at https://modis.gsfc.nasa.gov (accessed on 1 March 2022 and 14 March 2022). Zhengzhou POI data in 2020 were obtained from Gaode map (https://ditu.amap.com, accessed on 15 March 2022).

**Acknowledgments:** The authors thank the reviewers who provided valuable comments to improve the paper.

**Conflicts of Interest:** The authors declare no conflict of interest.

## References

1. Li, N.; Wu, H.; Luan, Q. Land surface temperature downscaling in urban area: A case study of Beijing. *Natl. Remote Sens. Bull.* **2021**, *25*, 1808–1820.
2. Zhu, J.; Zhu, S.; Yu, F.; Zhang, G.; Xu, Y. A downscaling method for ERA5 reanalysis land surface temperature over urban and mountain areas. *Natl. Remote Sens. Bull.* **2021**, *25*, 1778–1791.
3. Stone, B., Jr.; Vargo, J.; Liu, P.; Hu, Y.; Russell, A. Climate change adaptation through urban heat management in Atlanta, Georgia. *Environ. Sci. Technol.* **2013**, *47*, 7780–7786. [CrossRef]
4. Halder, B.; Bandyopadhyay, J.; Banik, P. Evaluation of the Climate Change Impact on Urban Heat Island Based on Land Surface Temperature and Geospatial Indicators. *Int. J. Environ. Res.* **2021**, *15*, 819–835. [CrossRef]
5. Voogt, J.A.; Oke, T.R. Thermal remote sensing of urban climates. *Remote Sens. Environ.* **2003**, *86*, 370–384. [CrossRef]
6. Lu, D.; Weng, Q. Use of impervious surface in urban land-use classification. *Remote Sens. Environ.* **2006**, *102*, 146–160. [CrossRef]
7. Wang, Z.; Sun, D.; Hu, C.; Wang, Y.; Zhang, J. Seasonal Contrast and Interactive Effects of Potential Drivers on Land Surface Temperature in the Sichuan Basin, China. *Remote Sens.* **2022**, *14*, 1292. [CrossRef]
8. Weng, Q.; Lu, D.; Schubring, J. Estimation of Land Surface Temperature–Vegetation Abundance Relationship for Urban Heat Island Studies. *Remote Sens. Environ.* **2004**, *89*, 467–483. [CrossRef]
9. Zhao, C.; Jensen, J.; Weng, Q.; Currit, N.; Weaver, R. Use of Local Climate Zones to investigate surface urban heat islands in Texas. *GIScience Remote Sens.* **2020**, *57*, 1083–1101. [CrossRef]
10. Zhao, C.; Jensen, J.; Weng, Q.; Currit, N.; Weaver, R. Application of airborne remote sensing data on mapping local climate zones: Cases of three metropolitan areas of Texas, US. *Comput. Environ. Urban Syst.* **2019**, *74*, 175–193. [CrossRef]
11. Biggart, M.; Stocker, J.; Doherty, R.M.; Wild, O.; Carruthers, D.; Grimmond, S.; Han, Y.; Fu, P.; Kotthaus, S. Modelling spatiotemporal variations of the canopy layer urban heat island in Beijing at the neighbourhood scale. *Atmos. Chem. Phys.* **2021**, *21*, 13687–13711. [CrossRef]
12. Streutker, D.R. Satellite-measured growth of the urban heat island of Houston, Texas. *Remote Sens. Environ.* **2003**, *85*, 282–289. [CrossRef]
13. He, B.; Zhao, Z.; Shen, L.; Wang, H.; Li, L. An Approach to Examining Performances of Cool/Hot Sources in Mitigating/Enhancing Land Surface Temperature under Different Temperature Backgrounds Based on Landsat 8 Image. *Sustain. Cities Soc.* **2019**, *44*, 416–427. [CrossRef]
14. Yang, J.; Zhan, Y.; Xiao, X.; Xia, J.C.; Sun, W.; Li, X. Investigating the Diversity of Land Surface Temperature Characteristics in Different Scale Cities Based on Local Climate Zones. *Urban Clim.* **2020**, *34*, 100700. [CrossRef]
15. Roy, S.; Pandit, S.; Eva, E.A.; Bagmar, M.S.H.; Papia, M.; Banik, L.; Dube, T.; Rahman, F.; Razi, M.A. Examining the nexus between land surface temperature and urban growth in Chattogram Metropolitan area of Bangladesh using long term Landsat series data. *Urban Clim.* **2020**, *32*, 100593. [CrossRef]

16. Hough, I.; Just, A.C.; Zhou, B.; Dorman, M.; Lepeule, J.; Kloog, I. A multi-resolution air temperature model for France from MODIS and Landsat thermal data. *Environ. Res.* **2020**, *183*, 109244. [CrossRef]
17. Xing, Z.; Li, Z.; Duan, S.; Liu, X.; Zheng, X.; Leng, P.; Gao, M.; Zhang, X.; Shang, G. Estimation of daily mean land surface temperature at global scale using pairs of daytime and nighttime MODIS instantaneous observations. *ISPRS J. Photogramm. Remote Sens.* **2021**, *178*, 51–67. [CrossRef]
18. Wu, W.; Li, L.; Li, C. Seasonal variation in the effects of urban environmental factors on land surface temperature in a winter city. *J. Clean. Prod.* **2021**, *299*, 126897. [CrossRef]
19. Wei, B.; Bao, Y.; Yu, S.; Yin, S.; Zhang, Y. Analysis of land surface temperature variation based on MODIS data a case study of the agricultural pastural ecotone of northern China. *Int. J. Appl. Earth Obs. Geoinf.* **2021**, *100*, 102342. [CrossRef]
20. Li, L.; Zha, Y.; Zhang, J. Spatially Non-Stationary Effect of Underlying Driving Factors on Surface Urban Heat Islands in Global Major Cities. *Int. J. Appl. Earth Obs. Geoinf.* **2020**, *90*, 102131. [CrossRef]
21. Wicht, M.; Wicht, A.; Osińska-Skotak, K. Detection of ventilation corridors using a spatiotemporal approach aided by remote sensing data. *Eur. J. Remote Sens.* **2017**, *50*, 254–267. [CrossRef]
22. Liu, D.; Zhou, S.; Wang, L.; Chi, Q.; Zhu, M.; Tang, W.; Zhao, X.; Xu, S.; Ye, S.; Lee, J.; et al. Research on the Planning of an Urban Ventilation Corridor Based on the Urban Underlying Surface Taking Kaifeng City as an Example. *Land* **2022**, *11*, 206. [CrossRef]
23. Yao, L.; Sun, S.; Song, C.; Li, J.; Xu, W.; Xu, Y. Understanding the spatio-temporal pattern of the urban heat island footprint in the context of urbanization, a case study in Beijing, China. *Appl. Geogr.* **2021**, *133*, 102496. [CrossRef]
24. Zhou, S.; Wang, K.; Yang, S.; Li, W.; Zhang, Y.; Zhang, B.; Fu, Y.; Liu, X.; Run, Y.; Chubwa, O.; et al. Warming Effort and Energy Budget Difference of Various Human Land Use Intensity: Case Study of Beijing, China. *Land* **2020**, *9*, 280. [CrossRef]
25. Wang, Z.; Meng, Q.; Allam, M.; Hu, D.; Zhang, L.; Menenti, M. Environmental and anthropogenic drivers of surface urban heat island intensity: A case-study in the Yangtze River Delta, China. *Ecol. Indic.* **2021**, *128*, 107845. [CrossRef]
26. Xiong, Y.; Zhang, F. Effect of human settlements on urban thermal environment and factor analysis based on multi-source data: A case study of Changsha city. *J. Geogr. Sci.* **2021**, *31*, 819–838. [CrossRef]
27. Liu, Y.; Yuan, Z.; Kong, W.; Sun, B.; An, B. The Changing Trend of Heat Island Intensity and Main Influencing Factors during 1993–2012 in Xi'an City. *J. Nat. Resour.* **2015**, *30*, 974–985.
28. Zhao, C.; Jensen, J.; Weng, Q.; Weaver, R. A Geographically Weighted Regression Analysis of the Underlying Factors Related to the Surface Urban Heat Island Phenomenon. *Remote Sens.* **2018**, *10*, 1428. [CrossRef]
29. Giannaros, T.M.; Melas, D. Study of the urban heat island in a coastal Mediterranean City: The case study of Thessaloniki, Greece. *Atmos. Res.* **2012**, *118*, 103–120. [CrossRef]
30. Tian, L.; Lu, J.; Li, Y.; Bu, D.; Liao, Y.; Wang, J. Temporal characteristics of urban heat island and its response to heat waves and energy consumption in the mountainous Chongqing, China. *Sustain. Cities Soc.* **2021**, *75*, 103260. [CrossRef]
31. Teri, K.; Sian, P.; Diana, B.; Amy, H.; Sian, K.; Ko, K.; Lorena, R. How effective is 'greening' of urban areas in reducing human exposure to ground-level ozone concentrations, UV exposure and the 'urban heat island effect'? An updated systematic review. *Environ. Evid.* **2021**, *10*, 1–38.
32. Ma, Y.; Zhao, M.; Li, J.; Wang, J.; Hu, L. Cooling Effect of Different Land Cover Types: A Case Study in Xi'an and Xianyang, China. *Sustainability* **2021**, *13*, 1099. [CrossRef]
33. Yi, Y.; Shen, G.; Zhang, C.; Sun, H.; Zhang, Z.; Yin, S. Quantitative analysis and prediction of urban heat island intensity on urban-rural gradient: A case study of Shanghai. *Sci. Total Environ.* **2022**, *829*, 154264. [CrossRef]
34. Alibakhshi, Z.; Ahmadi, M.; Asl, M. Modeling Biophysical Variables and Land Surface Temperature Using the GWR Model: Case Study—Tehran and Its Satellite Cities. *J. Indian Soc. Remote Sens.* **2020**, *48*, 59–70. [CrossRef]
35. Mohd, S.; Mohd, R.; Naikoo, W.; Ali, M.; Usmani, T.; Rahman, A. Urban Heat Island Dynamics in Response to Land-Use/Land-Cover Change in the Coastal City of Mumbai. *J. Indian Soc. Remote Sens.* **2021**, *49*, 2227–2247.
36. Liu, X.; Ming, Y.; Liu, Y.; Yue, W.; Han, G. Influences of landform and urban form factors on urban heat island: Comparative case study between Chengdu and Chongqing. *Sci. Total Environ.* **2022**, *820*, 153395. [CrossRef] [PubMed]
37. Wang, J.; Liu, J.; Wang, Y.; Liao, Z.; Sun, P. Spatiotemporal variations and extreme value analysis of significant wave height in the South China Sea based on 71-year long ERA5 wave reanalysis. *Appl. Ocean Res.* **2021**, *113*, 102750. [CrossRef]
38. Rahaman, Z.; Kafy, A.; Saha, M.; Rahim, A.; Almulhim, A.; Rahaman, S.; Fattah, M.; Rahman, M.; Kalaivani, S.; Faisal, A.; et al. Assessing the impacts of vegetation cover loss on surface temperature, urban heat island and carbon emission in Penang city, Malaysia. *Build. Environ.* **2022**, *222*, 109335. [CrossRef]
39. Zhao, Y.; Wu, Q.; Wei, P.; Zhao, H.; Zhang, X.; Pang, C. Explore the Mitigation Mechanism of Urban Thermal Environment by Integrating Geographic Detector and Standard Deviation Ellipse (SDE). *Remote Sens.* **2022**, *14*, 3411. [CrossRef]
40. Zhao, H.; Zhang, H.; Miao, C.; Ye, X.; Min, M. Linking Heat Source–Sink Landscape Patterns with Analysis of Urban Heat Islands: Study on the Fast-Growing Zhengzhou City in Central China. *Remote Sens.* **2018**, *10*, 1268. [CrossRef]
41. Geeta, S.J.; Payal, M. Assessment of seasonal climate transference and regional influential linkages to land cover–Investigation in a river basin. *J. Atmos. Sol.-Terr. Phys.* **2020**, *199*, 105209.
42. Mostafa, A.M.; Gamal, S.E.A.; Mohamed, E.E. Impact of climate change on rainfall variability in the Blue Nile basin. *Alex. Eng. J.* **2021**, *61*, 3265–3275.
43. Zhu, M.; Liu, D.; Tang, W.; Chi, Q.; Zhao, X.; Xu, S.; Ye, S.; Wang, Y.; Cui, Y.; Zhou, S. Exploring the Ecological Climate Effects Based on Five Land Use Types: A Case Study of the Huang-Huai-Hai River Basin in China. *Land* **2022**, *11*, 265. [CrossRef]

44. Li, W.; Yang, J.; Li, X.; Zhang, J.; Li, S. Extraction of urban impervious surface information from TM image. *Remote Sens. Nat. Resour.* **2013**, *25*, 66–70.
45. Hou, Y.; Ding, W.; Liu, C.; Li, K.; Cui, H.; Liu, B.; Chen, W. Influences of impervious surfaces on ecological risks and controlling strategies in rapidly urbanizing regions. *Sci. Total Environ.* **2022**, *825*, 153823. [CrossRef]
46. He, J.; Zhang, H.; Su, H.; Zhou, X.; Chen, Q.; Xie, B.; You, T. Study on long-term change of global spectral surface albedo. *J. Atmos. Environ. Opt.* **2022**, *17*, 279–293.
47. Mao, X.; Zhang, L.; Mao, T.; Wang, Y.; Huang, J. Research on the Influence of Fund Based on Pearson Study of Fund Influence Based on Pearson Correlation Analysis and Regression Analysis Method. *J. Zhejiang Sci-Tech Univ. (Soc. Sci. Ed.)* **2017**, *38*, 306–311.
48. He, P.; Chen, H.; Li, H.; Xi, W. Grey analysis of the urban heat island effect factors of the medium-sized city of Chuxiong on Yunnan Plateau. *Prog. Geogr.* **2009**, *28*, 25–32.
49. Li, X.; Zhang, H.; Qu, Y. Land Surface Albedo Variations in Sanjiang Plain from 1982 to 2015: Assessing with GLASS Data. *Chin. Geogr. Sci.* **2020**, *30*, 876–888. [CrossRef]
50. Gao, T.; Shen, R.; Li, L.; Wang, Y.; Huang, A. Spatial and Temporal Variations of Land Surface Albedo and Its Influencing Factors Based on MODIS Data. *Clim. Environ. Res.* **2021**, *26*, 648–662.
51. Feng, Y.; Hong, Z.; Cheng, J.; Jia, L.; Tan, J. Low Carbon-Oriented Optimal Reliability Design with Interval Product Failure Analysis and Grey Correlation Analysis. *Sustainability* **2017**, *9*, 369. [CrossRef]
52. Guo, J.; Dong, Y.; Zhang, H. Misuse of gray incidence analysis in variable selection. *Syst. Eng. Theory Pract.* **2002**, *22*, 126–128.
53. He, W.; Cao, S.; Du, M.; Hu, D.; Mo, Y.; Liu, M.; Zhao, J.; Cao, Y. How Do Two- and Three-Dimensional Urban Structures Impact Seasonal Land Surface Temperatures at Various Spatial Scales? A Case Study for the Northern Part of Brooklyn, New York, USA. *Remote Sens.* **2021**, *13*, 3283. [CrossRef]
54. Chang, Y.; Xiao, J.; Li, X.; Zhou, D.; Wu, Y. Combining GOES-R and ECOSTRESS land surface temperature data to investigate diurnal variations of surface urban heat island. *Sci. Total Environ.* **2022**, *823*, 153652. [CrossRef] [PubMed]
55. Maryam, M.; Masoud, M.; Zarkesh, K.; Alireza, M.; Ali, J. Achieving sustainable development goals through the study of urban heat island changes and its effective factors using spatio-temporal techniques: The case study (Tehran city). In *Natural Resources Forum*; Blackwell Publishing Ltd.: Oxford, UK, 2022; Volume 46, pp. 88–115.